Markl, Daniel ; Wang, Parry; Ridgway, Cathy; Karttunen, Anssi Pekka; Chakraborty, Mousumi; Bawuah, Prince; Pääkkönen, Pertti; Gane, Patrick; Ketolainen, Jarkko; Peiponen, Kai-Erik; Zeitler, J. Axel

Characterization of the Pore Structure of Functionalized Calcium Carbonate Tablets by Terahertz Time-Domain Spectroscopy and X-Ray Computed Microtomography

Please cite the original version:
Markl, D., Wang, P., Ridgway, C., Karttunen, A. P., Chakraborty, M., Bawuah, P., Pääkkönen, P., Gane, P., Ketolainen, J., Peiponen, K.-E., & Zeitler, J. A. (2017). Characterization of the Pore Structure of Functionalized Calcium Carbonate Tablets by Terahertz Time-Domain Spectroscopy and X-Ray Computed Microtomography. *Journal of Pharmaceutical Sciences*, *106*(6), 1586–1595. https://doi.org/10.1016/j.xphs.2017.02.028

Pharmaceutics, Drug Delivery and Pharmaceutical Technology

Characterization of the Pore Structure of Functionalized Calcium Carbonate Tablets by Terahertz Time-Domain Spectroscopy and X-Ray Computed Microtomography

Daniel Markl [1], Parry Wang [1], Cathy Ridgway [2], Anssi-Pekka Karttunen [3], Mousumi Chakraborty [4], Prince Bawuah [4], Pertti Pääkkönen [4], Patrick Gane [2, 5], Jarkko Ketolainen [3], Kai-Erik Peiponen [4], J. Axel Zeitler [1, *]

[1] Department of Chemical Engineering and Biotechnology, University of Cambridge, Cambridge, UK
[2] Omya International AG, Oftringen, Switzerland
[3] School of Pharmacy, Promis Centre, University of Eastern Finland, Kuopio, Finland
[4] Institute of Photonics, University of Eastern Finland, Joensuu, Finland
[5] Department of Bioproducts and Biosystems, School of Chemical Engineering, Aalto University, Aalto, Helsinki, Finland

ARTICLE INFO

ABSTRACT

Novel excipients are entering the market to enhance the bioavailability of drug particles by having a high porosity and, thus, providing a rapid liquid uptake and disintegration to accelerate subsequent drug dissolution. One example of such a novel excipient is functionalized calcium carbonate, which enables the manufacture of compacts with a bimodal pore size distribution consisting of larger interparticle and fine intraparticle pores. Five sets of functionalized calcium carbonate tablets with a target porosity of 45%-65% were prepared in 5% steps and characterized using terahertz time-domain spectroscopy and X-ray computed microtomography. Terahertz time-domain spectroscopy was used to derive the porosity using effective medium approximations, that is, the traditional and an anisotropic Bruggeman model. The anisotropic Bruggeman model yields the better correlation with the nominal porosity ($R^2 = 0.995$) and it provided additional information about the shape and orientation of the pores within the powder compact. The spheroidal (ellipsoids of revolution) shaped pores have a preferred orientation perpendicular to the compaction direction causing an anisotropic behavior of the dielectric porous medium. The results from X-ray computed microtomography confirmed the nonspherical shape and the orientation of the pores, and it further revealed that the anisotropic behavior is mainly caused by the interparticle pores. The information from both techniques provides a detailed insight into the pore structure of pharmaceutical tablets. This is of great interest to study the impact of tablet microstructure on the disintegration and dissolution performance.

© 2017 The Authors. Published by Elsevier Inc. on behalf of the American Pharmacists Association®. This is an open access article under the CC BY license (http://creativecommons.org/licenses/by/4.0/).

Introduction

Overall in the pharmaceutical market, tablets continue to be the most convenient way to deliver an active pharmaceutical ingredient (API) to the patient. In industrial practice, the tableting and delivery functionality of a formulation are dominated by the physical and chemical properties of the excipients and API particles, and in most cases, the excipients represent by far the greater quantity in a tablet compared with API. Therefore, it is not surprising that they play a crucial role in defining the ease of tableting and in improving the disintegration and dissolution performance of the dosage form.[1,2] The design of targeted drug release requires specialist development of functional excipients, for example, to provide rapid oral dispersibility or to prolong the drug release.

Due to its good flowability and excellent compressibility, one of the most commonly used of such excipients is microcrystalline cellulose (MCC). Additionally, and very importantly for its

---

functionality, MCC absorbs water, both into the interparticulate pore structure[3,4] and by diffusion into the cellulose intraparticle space.[5] Together with the excellent surface wetting properties by water, this makes MCC an excipient for a broad spectrum of applications ranging from orally dispersible tablets[6] to controlled drug delivery.[7] However, its use in orally dispersible tablets is constrained due to its limited capability of achieving tablet porosities >40%. High porosities are desirable as the pore structure of a tablet have strong impact on the liquid penetration in a tablet, which is in the majority of cases the limiting step during disintegration. Furthermore, poor solubility in gastric fluids is a common problem for newly developed drug candidates. Effective disintegration of a tablet is, thus, critical in maximizing the exposure time of the API to gastric and intestinal fluids so that the API can be absorbed at higher rates, leading to increased bioavailability and a faster onset of the desired pharmacologic effect.

To overcome the limitation in terms of the maximum achievable porosity, porous particle excipients are being developed to enhance liquid imbibition and, hence, the disintegration and dissolution performance. Such a novel excipient is functionalized calcium carbonate (FCC), which has a very high intraparticle porosity to facilitate rapid liquid uptake. Compacts of this excipient, therefore, display a discretely separable bimodal pore size distribution, composed of larger interparticle and fine intraparticle pores.[8] If the formulation or tableting process requires it, the particles can be agglomerated or granulated providing an additional even larger pore size region associated with intergranulate pores. This new generation of excipient was shown to be particularly effective in forming resilient tablets at low density and *in vitro* ultra-rapid tablet dissolution, exceeding the rate seen with MCC by typically a factor of 10.[9] The performance of such tablets, thus, strongly depends on the pore structure, which is commonly characterized by the porosity, that is, the ratio between the void volume and the bulk volume.

Terahertz time-domain spectroscopy (THz-TDS) has recently emerged as a promising analytical tool for the characterization of pharmaceutical materials to analyze the pore structure and quantify its porosity. The terahertz domain (100 GHz to 3 THz) lies in between the infrared and microwave regions within the electromagnetic spectrum. Compared with NIR, mid-IR, and Raman spectroscopy, THz-TDS is inherently less vulnerable to scattering effects due to its longer wavelength (100 μm to 3 mm) and it is, therefore, a very attractive technique to characterize porous pharmaceutical tablets, such as FCC powder compacts.

In THz-TDS, pharmaceutical tablets are characterized on the basis of their effective refractive index, n_{eff}, which is then used to calculate the porosity of the powder compacts in combination with effective medium theory. Effective medium approximations (EMAs) were developed extensively during the last century to model the effective permittivity, ε_{eff}, of porous media based on the Maxwell-Garnett[10] and the Bruggeman[11] formalisms. The Maxwell-Garnett approximation is only valid for a low-volume fraction of inclusions, whereas the Bruggeman formalism can be applied to approximate the effective medium for highly porous systems.

In previous studies, the traditional Bruggeman model was used to predict the porosity (up to approximately 40%) of MCC powder compacts,[12] and it was assumed that the pore shape can be approximated by a spherical geometry. These assumptions, however, may not be valid for all pharmaceutical powder compacts as discussed in this study. We applied a modification of the traditional Bruggeman model[13] to account for nonspherical pore shapes and compared this with the traditional approach. Furthermore, the terahertz measurements can provide additional information about the pore arrangement by calculating the so-called *S* parameter, which considers the pore network as a

combination of pore components in series and parallel assembly.[14] The results from the terahertz measurements are complemented and compared with characteristic pore structure parameters extracted from X-ray computed microtomography (XμCT). The XμCT analysis specifically focused on characterizing the orientation and shape of the pores, which were compared with the results from the terahertz measurements. These methodologies were studied for 5 different sets of tablets with porosity levels ranging from 45% to 65%.

Materials and Methods

Materials

The powder compacts used in this study consisted of FCC (Omyapharm®; Omya International AG, Oftringen, Switzerland) particles. FCC is a shell-core structure of lamellar hydroxyapatite surrounding agglomerated ultrafine calcium carbonate particulates, respectively. This is formed in a process whereby the surfaces of calcium carbonate particles are etched and then re-precipitated to create a highly porous plate-like, nanometre thick lamellar structure of high surface area. A typical pharmaceutical FCC particle consists of a calcium carbonate/hydroxyapatite ratio of 15%-20% calcium carbonate to 80%-85% hydroxyapatite.

The FCC powder was directly compressed into flat-faced, cylindrical tablets with target thicknesses of 1.5 mm and target diameters of 10 mm using a compaction simulator (PuuMan Ltd, Kuopio, Finland). Given the highly porous nature of the FCC particles, it was possible to manufacture tablets with target total porosities of 45%-60% with 5% increments. The batches were labeled as B01-B05 (low to high porosity) as listed in Table 1 and each batch consisted of 15 tablets.
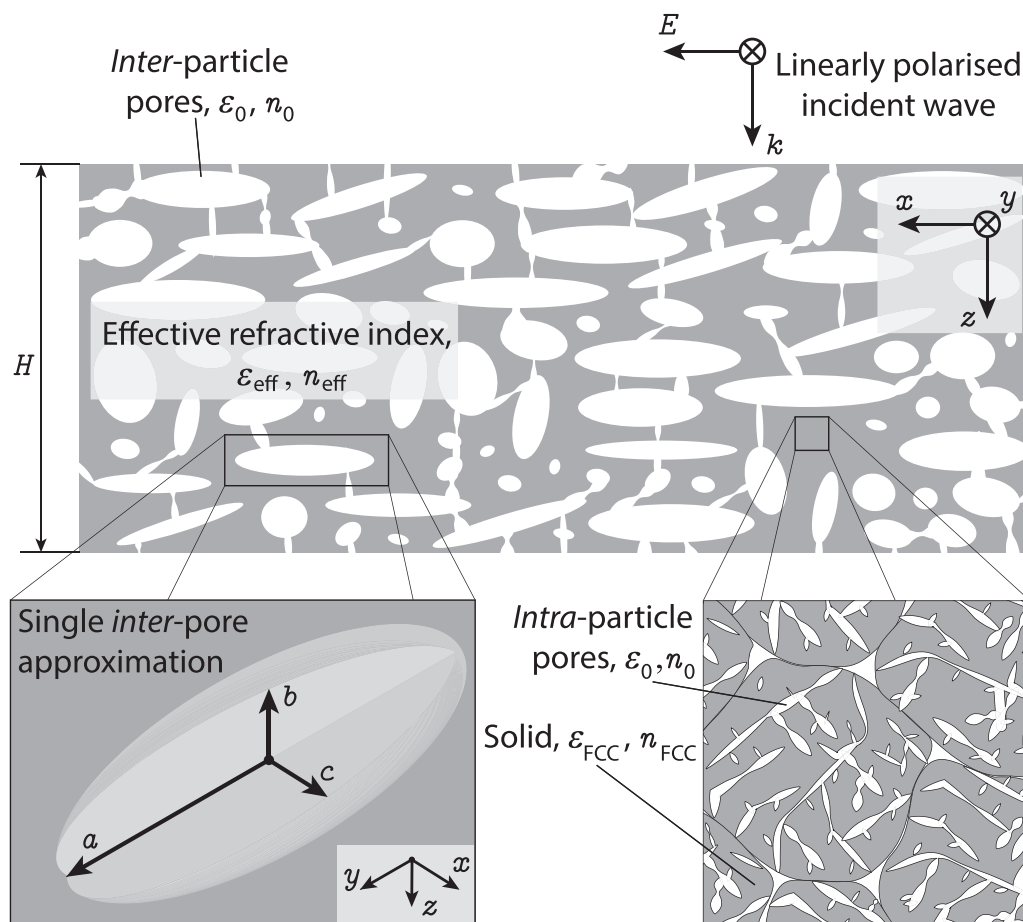
Mass (m), thickness (H), and diameter (D) of each tablet were measured using a precision balance (Ohaus Corp., Parsippany, NJ) and a micrometer (Expert Metric External Micrometer 0-25 mm; Draper Expert, Hampshire, UK) with measurement uncertainties of $\pm$0.1 mg and $\pm$1 μm, respectively. The porosity (henceforth referred to as the nominal porosity) can be calculated by

$$f_{nominal} = \left(1 - \frac{4m}{\pi D^2 H \varrho_{true}}\right) \qquad (1)$$

with $\varrho_{true} = 2.958 \pm 0.062$ g cm^{-3} (5 repeats) as the true density of FCC. The true density of FCC powder was measured with a helium pycnometer (Multipycnometer MVP-1; Quantachrome Corporation, New York, NY). Before the measurement, volatile contaminants were removed by degassing the sample by a helium purge.

Terahertz Time-Domain Spectroscopy

Terahertz time-domain (TD) measurements were acquired using a Terapulse 4000 spectrometer (Teraview Ltd., Cambridge,

Table 1
List of Batches Characterized in This Study

Code	Mass	Thickness	Diameter	Porosity
	m, mg	H, mm	D, mm	$f_{nominal}$, %
B01	217 $\pm$ 2	1.67	10.04	45.50 $\pm$ 0.52
B02	190 $\pm$ 2	1.64	10.03	50.27 $\pm$ 0.50
B03	168 $\pm$ 2	1.63	10.02	55.72 $\pm$ 0.40
B04	147 $\pm$ 3	1.62	10.02	61.02 $\pm$ 0.93
B05	122 $\pm$ 3	1.61	10.00	67.35 $\pm$ 0.79

Each batch consisted of 15 tablets. The SD of the thickness and diameter measurements were all <10 μm.

Figure 1. Schematic of the tablet exposed to a linearly polarized terahertz wave. *k* is the unit vector in the direction of propagation of the horizontally (parallel to the *y*-axis) linear-polarized incident terahertz wave. The tablet which consists of intra- and interparticle pores with the permittivity of ambient air ($\varepsilon_0 = n_0^2 = 1$). The intrinsic permittivity and refractive index of the skeletal material of an FCC particle are defined as ε_{FCC} and n_{eff}, respectively.

UK) in a transmission setup. The transmission chamber was purged with dry nitrogen gas throughout the measurement and the noise reduced by co-averaging 60 measurements. Each TD waveform covered a range of 150 ps using a resolution of 0.1 ps, and the total measurement time of the co-averaged waveforms was 1.5 min.

The effective refractive index, n_{eff}, of a sample can be calculated from terahertz TD measurements either by simply comparing a reference waveform (i.e., no sample present in the measurement chamber) and the sample waveform in the TD or by transforming the waveforms in the frequency-domain (FD) and applying Beer-Lambert's law. In case of the TD analysis, the effective refractive index (n_{eff}) of the tablet is related to the pulse delay (Δt) by

$$\Delta t = \frac{H\left(n_{eff} - n_0\right)}{c}, \tag{2}$$

where c is the speed of light in vacuo and $n_0 = 0$ is taken to approximate the refractive index of ambient air ($n = 1.0003$).

n_{eff} and the effective absorption coefficient, α_{eff}, of each tablet can also be determined in the FD. The terahertz waveforms of the reference and the sample are transformed to the FD by a fast Fourier transform. The frequency-dependent n_{eff} and α_{eff} are then calculated by assuming the tablet as a homogeneous medium. The n_{eff} evaluated at one specific frequency can then be used to calculate the tablet porosity as discussed in the next section.

Pore Structure Analysis Using THz-TDS

The porosity of a sample can be determined from n_{eff}, which was calculated either in TD or in FD. This can be performed by applying the zero porosity approximation (ZPA) or using models from the effective medium theory, where the pores and the solid matrix, that is, skeletal material forming the pore walls in the FCC powder are considered as the dispersed and the continuous phase, respectively. In general, the porosity determined by THz-TDS captures the intraparticle pores and the interparticle pores, where both void spaces include open and closed pores, if the latter also exists.

Zero Porsosity Approximation

ZPA is a linear extrapolation technique, which relates n_{eff} and the porosity of the tablet by assuming a linear relationship between the 2 variables. For tablets with only 1 component, FCC, the following equation applies[12,15]

$$n_{eff}(f) = n_{FCC} + (1 - n_{FCC})f, \tag{3}$$

n_{FCC} is the intrinsic refractive index of FCC, which can be determined using the n_{eff} of samples with known porosity. We want to stress here that n_{FCC} refers to the skeletal material of the FCC particle, that is, without the intraparticle pores, as illustrated in the inset of Figure 1. The porosity can be calculated from different information, the method of which is given in the subscript of

f throughout this article. ZPA can also be used to predict the porosity for a known n_{eff} by rearranging Equation 3.

Bruggeman Model

Polder and van Santen[13] introduced the concept of a depolarization factor, L, to consider the effect of a nonspherical shape of the inclusions. They approximated inclusions as spheroids (ellipsoids of revolution), which have a unique major axis a and 2 common minor axes b and c, as illustrated in Figure 1. The terahertz measurements were conducted by focusing the linearly polarized terahertz radiation onto the tablet face, and therefore, ε_{eff} was only measured when the electric field, E, was aligned in parallel with the x-axis. In general, the anisotropic Bruggeman model, AB-EMA, for a 2-component system can be expressed as[16]

$$\left(\frac{\varepsilon_a - \varepsilon_{eff}}{\varepsilon_{eff} + L\left(\varepsilon_a - \varepsilon_{eff}\right)}\right)f_a + \left(\frac{\varepsilon_b - \varepsilon_{eff}}{\varepsilon_{eff} + L\left(\varepsilon_b - \varepsilon_{eff}\right)}\right)f_b = 0. \tag{4}$$

f_a and f_b are the volume fractions of component a (skeletal fraction of the FCC material in the particulate powder) and b (air), which are substituted by $f_a = 1 - f$ (solid fraction) and $f_b = f$ (porosity) in this study. The intrinsic permittivities are substituted by $\varepsilon_a = \varepsilon_{FCC}$ and $\varepsilon_b = 1$. ε_{FCC} and n_{FCC} correspond to the optical properties of the skeletal material of an FCC particle, and this definition is used throughout this study whenever we refer to the intrinsic permittivity, intrinsic refractive index, an FCC particle, or FCC powder. Setting $L = 1/3$ yields the traditional Bruggeman model (henceforth referred to as TB-EMA) as it was used in the past to model pharmaceutical tablets.[17]

Determination of a Structural Parameter

Recently, Bawuah et al.[14] proposed a structural parameter (S parameter), which is based on Wiener bounds and the n_{eff} of a porous medium. The Wiener bounds for ε_{eff} of a porous medium are determined by considering the constituents within the tablet as equivalent to different dielectrics in parallel and series connection within a capacitor and dealing with the total capacitance. The upper and lower Wiener bounds, n_U and n_L, are the 2 extreme cases when both constituents (FCC powder and air) are either in series or in parallel connection. Assuming the absence or presence of only weak absorption of terahertz waves by the material under investigation, the Wiener bounds can be expressed as

$$n_U = \sqrt{f + (1-f)n_{FCC}^2}, \tag{5}$$

$$n_L = \sqrt{\frac{1}{f} + \frac{1-f}{n_{FCC}^2}}. \tag{6}$$

By making no assumptions about the shape of the microstructures in the porous medium and treating the problem analogous to heat conduction, S can be expressed as

$$S = \frac{1}{n_U^2 - n_L^2}\left(\frac{n_U^2 n_L^2}{n_{eff}^2} - n_L^2\right). \tag{7}$$

Pore Structure Analysis Using X-Ray Computed Microtomography

The pore structure was analyzed by acquiring high-resolution 3D data of 4 FCC tablets using XμCT. A SkyScan 1172 (Bruker, Antwerp, Belgium) was used to image the samples with an isotropic voxel size of 0.47 μm. This instrument uses a cone beam geometry and a 2-dimensional array detector. The object is rotated through 180° with steps of 0.25°. The actual 3-dimensional (3D) data were reconstructed using NRecon (v1.6.8.0; Bruker) and further processed with Avizo Fire as proposed in Markl et al.[18] for the analysis of 3D printed tablets. The pore network is extracted from the XμCT data by thresholding and a marker-controlled watershed algorithm using defined foreground and background regions. The watershed algorithm generates a topographical map from the image gradient and so detects catchment basins and watershed ridge lines. These data are then used to separate touching pores and to assign each voxel in the pore space to the relevant specific pore. The pore volume is, thus, always a multiple of the voxel volume (0.47^3 mm^3).

Pore Structure Analysis Using Mercury Porosimetry

An Autopore V mercury porosimeter (Micromeritics Instrument Corporation, Norcross, GA) was used to perform mercury intrusion measurements. Mercury porosimetry measurements were conducted for the FCC powder to determine the intraparticle porosity and for 1 compacted tablet per batch to analyze the pore size distributions.

Roughness Analysis

Several studies have already demonstrated the characterization of the surface roughness of pharmaceutical tablets with the aid of a laser stylus.[17,19-21] A noncontact optical interference profilometer (WYKO NT9300; Veeco, Plainview, NY) was used to quantify the average surface roughness, R_a, of the FCC tablets. The principle of the profilometer was presented in detail in Bawuah et al.[17]

Results

Terahertz Time-Domain Spectroscopy

Since all tablets were compacted to the same target thickness, the measured pulse delay difference, Δt, between the terahertz sample and reference waveforms and the effective refractive index depend linearly on the nominal porosity, $f_{nominal}$ (Fig. 2). Therefore, both Δt and n_{eff} decrease with increasing porosity.

The frequency-dependent n_{eff} is shown in Figure 3 and α_{eff} is presented in the Supporting Information. No peaks are observed in α_{eff} indicating the absence of phonon vibrations in FCC at terahertz frequencies. Moreover, the long wavelength (100 μm-3 mm) of the terahertz radiation obviates the need to consider Mie scattering because the particulate material size ($\leq$5 μm), in its primary form, lies below the scattering limit for this wavelength region.

The intrinsic refractive index of FCC, n_{FCC}, can be extracted using ZPA (Eq. 3), TB-EMA (Eq. 4 with $L = 1/3$), or AB-EMA (Eq. 4) on the basis of n_{eff} determined in TD or in FD. The porosity predictions of the TB-EMA are affected by a systematical error as observable in Figure 4a. This deviation from the nominal porosity is due to the strong dependence of n_{FCC} on the porosity (Fig. 4b), which indicates that the assumption of spherical shaped inclusions as made by the TB-EMA is not valid for the FCC powder compacts. Therefore, the FCC tablets are anisotropic porous media exhibiting different ε_{eff} when measured in the axial or radial direction of the tablet. The AB-EMA can account for effects of pore shapes by considering the pores as spheroids (see inset in Fig. 1). Therefore, a depolarization factor was estimated as $L = 0.21$ using iterative least square fitting, which renders the intrinsic refractive index independent of the porosity (open circles in Fig. 4). L is related to the aspect ratio of the unique axis a and the 2 common axes $b = c$ of the spheroid by Jones and Friedman[22]
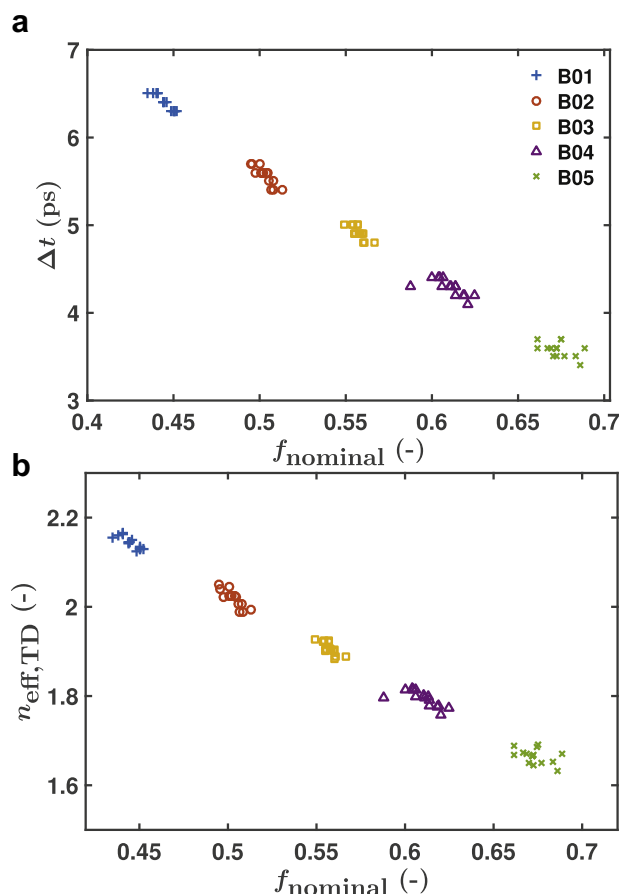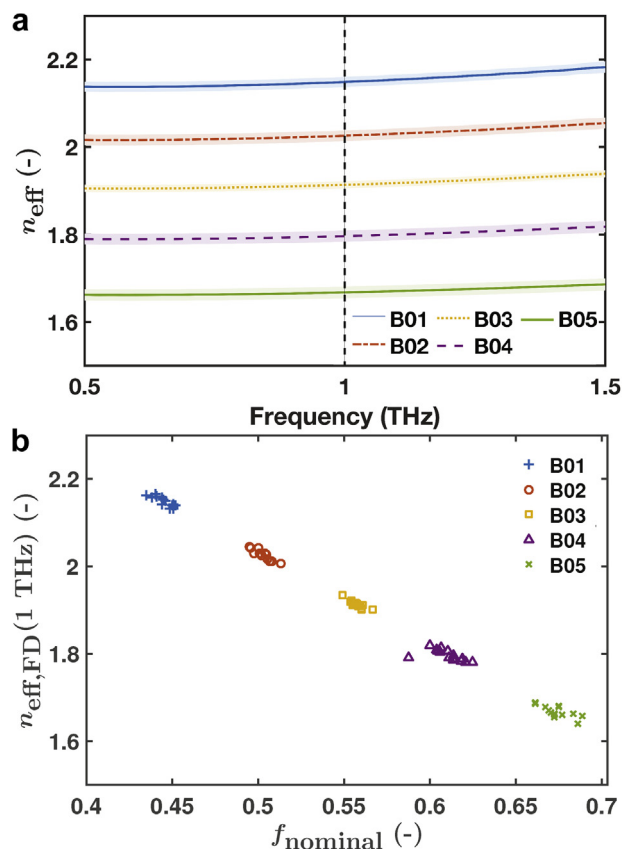
Figure 2. (a) Pulse delay difference, Δt, and (b) effective refractive index, n_{eff}, as a function of the nominal porosity (Eq. 1). n_{eff} is calculated by using Equation 2 under consideration of the measured thickness of each tablet.


Figure 3. Effective refractive as a function of (a) frequency and (b) the nominal porosity. In (a), the solid lines are the average for each batch and the shaded area corresponds to the SD within each batch. In (b), the effective refractive index was evaluated at 1 THz.

$$L = \frac{1}{1 + 1.6(a:b) + 0.4(a:b)^2}. \qquad (8)$$

$L = 0.21$, thus, yields an aspect ratio, $a:b$, of 1.7. Although the pore shape derived from the depolarization factor is only a rough approximation of the actual geometry, it evidences a nonspherical pore shape with a preferred major axis perpendicular to the compaction direction. It is important to note that the assignment of the axes x and y (see Fig. 1) is arbitrary, and therefore, we cannot analyze the orientation of irregularly shaped pores around the z-axis using the current concept. However, the absence of birefringence and, thus, absence of any anisotropic behavior in the x-y plane, was experimentally verified by rotating 1 FCC tablet of each batch over 315° at 45° increments around z-axis and performing a terahertz measurement at every step. The changes between the 8 measurements of every tablet were below the resolution of the used terahertz setup, and therefore, no anisotropic effect in the x-y plane could be observed. The results of XμCT also support this finding by revealing that there is no preferred orientation of the pores around the z-axis (see Fig. S5 in the Supporting Information).

The statistical analysis of the different models as summarized in Table 2 emphasizes that the AB-EMA using from the FD analysis is more favorable compared with the other approaches. The ZPA (data are provided in the Supporting Information) is also highly applicable for the tablets used in this study due to the fact that it does not make any assumption of a specific shape of the pores. Therefore, the porosity calculations from both methods are highly

accurate, but ZPA does not provide any information about the pore shape. The high correlation of the porosity calculations from both methods confirms the assumption made for the AB-EMA on the shape of the pores, and it particularly highlights the high level of confidence of the depolarization factor from the AB-EMA. Moreover, the $n_{FCC} = 2.97$ (AB-EMA and FD) is in good agreement with the refractive index at terahertz frequencies for calcium carbonate as determined by Peiponen et al.[23] We want to remind the reader once again at this point that the intrinsic refractive index, n_{FCC}, refers to that of the skeletal material of an FCC particle, and thus, it does not include the intraparticle pores.

Furthermore, we assume for the interpretation of the results of the TB-EMA and AB-EMA that compacted FCC powder is not birefringent. Although calcium carbonate is birefringent in the form of a single crystal, we support the finding above of no linked measurable anisotropy about the rotational z-axis between structural and optical response by the assumption that the calcium carbonate crystallite domains are randomly oriented throughout the FCC structure due to the reconstituting process derived from many reacted original calcium carbonate microparticle building blocks. The very small size (≈ 10 nm) and the randomized orientation of the remaining calcium carbonate domains within each FCC particle, and the further randomization of the FCC particles in the compact, should, therefore, render birefringence of the powder compact immeasurably small.
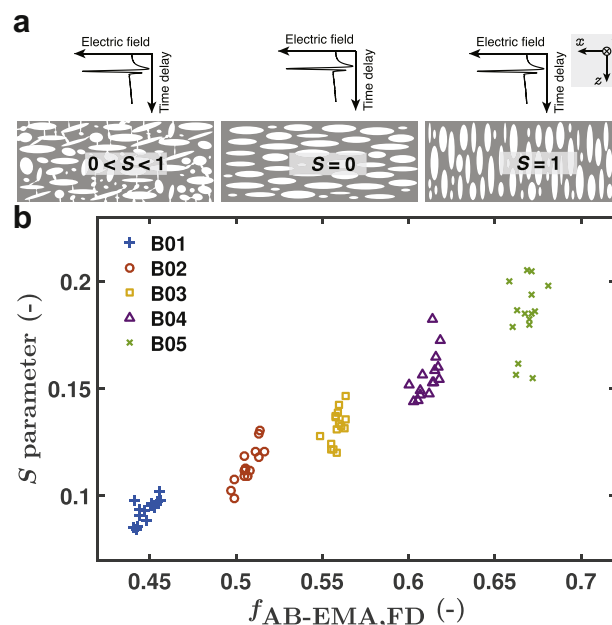
The change of the structural arrangement of pores can also be studied on the basis of the S parameter (Eq. 7). Although the pores are nonspherical, the S parameter can be used to analyze such samples as it is based on the Wiener bounds, which again do not
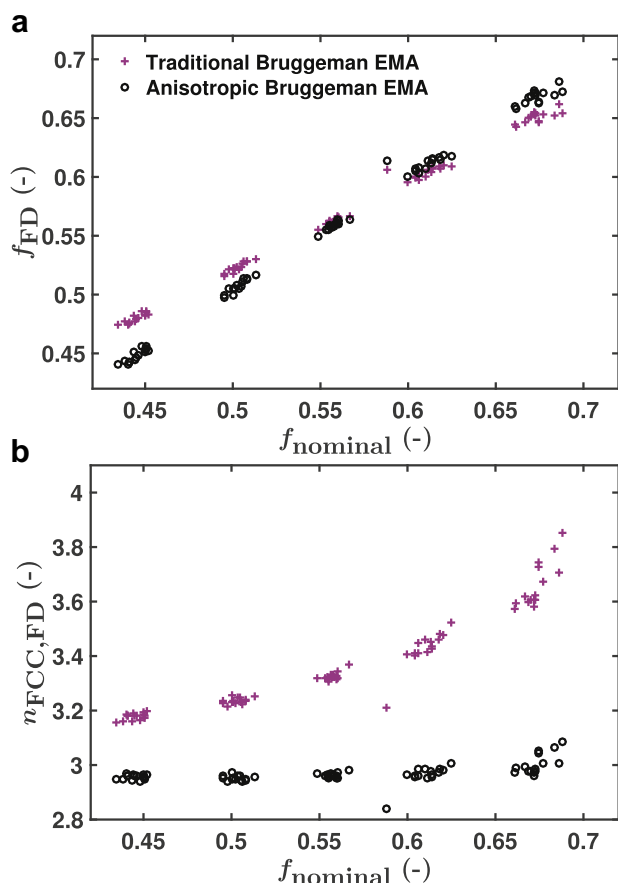
Figure 4. Comparison of the results from TB-EMA and AB-EMA. (a) The predicted porosity, f_{FD}, using n_{eff} determined by the FD analysis and (b) the intrinsic refractive indices, $n_{FCC,FD}$, calculated for each tablet separately are plotted as a function of the nominal porosity.

make any assumptions regarding the geometry and degree of isotropy.[24,25] The samples in this study only consist of one excipient, and thus, we can be sure that changes in the S parameter are purely related to structural variations of the pores. In general, the S parameter reflects changes in the structural arrangement of pores, where the extreme case of $S = 0$ corresponds to a series arrangement with respect to the compaction direction, as schematically illustrated in Figure 5a. The S parameter additionally depends on the porosity (Fig. 5b), which makes the interpretation of the structural changes on the basis of the S parameter more difficult. Further research is required to separate the influence from the porosity and from the structural arrangement of the pores on the S parameter.

The variance in the S parameter of each batch is significantly higher than that of the porosity, and it also increases with

Table 2
Comparison of the Results of ZPA (Eq. 3), TB-EMA (Eq. 4 With $L = 1/3$), and AB-EMA (Eq. 4)

Variable	TB-EMA		AB-EMA		ZPA	
	TD	FD	TD	FD	TD	FD
R^2	0.935	0.936	0.993	0.995	0.995	0.995
RMSE 10^{-3}	21.5	21.3	6.8	5.5	5.9	5.9
n_{FCC}	3.35	3.37	2.96	2.97	3.08	3.09

R^2 and the RMSE were calculated for the porosity predicted by the respective model and the nominal porosity. n_{eff} was determined for each model using n_{eff} from the TD and from the FD analysis.
RMSE = root mean squared error.

Figure 5. (a) Schematic for the interpretation of the S parameter. (b) S parameter as a function of porosity. The porosity was predicted from the AB-EMA using n_{eff} from the FD analysis. n_{FCC} (required for the calculation of the Wiener bounds in Eqs. 5 and 6) was calculated using AB-EMA and is given in Table 2.

increasing porosity, which clearly indicates that the S parameter reflects changes of the interparticle pore structure. Since all batches were manufactured from the same batch of FCC powder, the intraparticle pore structure is assumed to be very similar for all tablets and batches. The FCC particles have an inherent porosity of about 25%, and the intraparticle porosity, thus, strongly contributes to the total porosity of the powder compact. The porosity associated with the intraparticle pores was derived from mercury porosimetry measurements of the FCC powder. Therefore, the inherent porosity was calculated by multiplying the specific intraparticle pore volume with the bulk density of the measured powder (see Supporting Information for more details).

The porosity of tablets from batch B01 is particularly affected by the intraparticle pores, which also feature a very consistent arrangement of the pores as revealed by the small variations in the S parameter of these tablets. Therefore, the observed changes of the pore structure are primarily variations of the interparticle pores as the intraparticle pores were not affected by the compaction. The assumption that the intraparticle pores remain unchanged is supported by the mercury porosimetry data as discussed below.

Pore Structural Characterization by XμCT

Characteristic pore structural parameters from XμCT measurements are summarized in Table 3. Because the measured tablets from the same batch show almost identical values across the different parameters, we present in the following only the data of one tablet per batch. Unsurprisingly, the average porosity, equivalent diameter, pore volume, and pore length are larger for the tablets from B05 compared with those from B02. The porosity from the XμCT measurements is significantly lower than the nominal porosity (50% and 65% for B02 and B05, respectively).

Due to the intraparticle pores having a pore size distribution with its mean at 200 nm, a large portion of the intraparticle pores cannot be resolved using the XμCT technique given the resolution limit of 0.47 μm for the instrument in our laboratory. However, the

Table 3
Pore Structure Characteristics From XμCT Measurements

Variable	Porosity, %	Equivalent Diameter, μm	Pore Volume, 10^{-7} mm³	Pore Length, μm	Anisotropy
B02 - tablet 1	35.7	6.5 ± 4.3	3.2 ± 3.7	14.1 ± 10.0	0.71 ± 0.12
B02 - tablet 2	35.8	6.5 ± 4.3	3.2 ± 3.7	14.1 ± 10.0	0.71 ± 0.12
B05 - tablet 1	51.5	7.7 ± 9.0	17.5 ± 43.5	16.4 ± 20.5	0.73 ± 0.12
B05 - tablet 2	51.3	7.7 ± 9.0	17.9 ± 43.8	16.4 ± 20.7	0.73 ± 0.12

All parameters are given as the average values ± SD of all pores. The pore length is the maximum feret length measured in 3D. The anisotropy is calculated for each pore by $1 - \lambda_{min}/\lambda_{max}$ with λ_{min} and λ_{max} as the minimum and maximum eigenvalue, respectively. More details about the eigenvalues and eigenvectors are provided in Figure 7.

deviation from the actual porosity is only 15%, and thus, the XμCT measurement was able to capture a surprisingly large number of intraparticle pores. Moreover, the relative porosity difference between the 2 batches is in a very good agreement with the actual porosity difference of 15%.

The frequency distributions of the equivalent diameter and the pore length clearly show a bimodal pore size distribution caused by the intra- and interparticle pores (Fig. 6). The first mode of the pore size distributions is related to the intraparticle pores and is very similar between the different batches. The second mode corresponds to the interparticle pores, which was affected by the powder compaction. Although the second mode of both distributions is larger for the tablet with a lower porosity (B02), the higher porosity batch (B05) has a high number of very large and long interparticle pores. This analysis, thus, indicates that lower compaction pressure retains a combination of small interparticle pores and very large and long interparticle pores, both of which provide the greater overall porosity.

Because the size of the intra- and small interparticle pores is below or very close to the resolution limit of the used XμCT system, the level of confidence of pore-specific parameters for these pores is low. Therefore, we only considered interparticle pores (equivalent diameter >2.5 μm) in the following analysis of the anisotropy and orientation of the pores.

The XμCT data can also be analyzed to reveal the orientation and shape of the interparticle pores. The principal orientation is given by the eigenvector with the largest eigenvalue, and the ratios between the eigenvalues provide a shape descriptor of the pore. This analysis further confirms the nonspherical shape of the pores as reflected in the anisotropy (Table 3, Fig. 7, and Fig. 8a). The anisotropy value ranges from 0 (fully isotropic) to 1 (fully anisotropic), and the average value slightly increases for increasing porosity. Analyzing the orientation of the principal direction of a pore (Fig. 8b) reveals that a second mode is forming at 90°, which indicates that the main axis is perpendicular to the compaction direction. This is in agreement with the results from the THz-TDS using AB-EMA which considers the anisotropy of the powder compact.

Our results confirm previous reports that found that the tablet compaction process may cause anisotropy in the mechanical properties when measured in parallel (axial) or perpendicular (radial) to the compaction direction.[26-29] The compaction process is well known to result in a heterogeneous internal tablet structure due to confining the powder radially by a rigid die while compressing the tablet axially by the punch. Wu et al.[29] investigated the anisotropy in pore structure and the mechanical strength of cubic starch compacts. The results from this work already presented evidence that the pores were primarily oriented perpendicular to the direction of compression, which is in excellent agreement with our measurements on a different type of excipient using independent measurement techniques.

Pore Structure Analysis Using Mercury Porosimetry

Mercury porosimetry facilitates the determination of the pore size distribution of a pharmaceutical tablet (Fig. 9). Cumulative

pore intrusion volumes for the different tablets are presented in the Supporting Information. The results clearly reveal a bimodal pore size distribution as already discussed on the basis of the XμCT data. Although the results are qualitatively in good agreement, the pore sizes from mercury porosimetry are significantly smaller than those from XμCT. On the one hand, this discrepancy is due to the limited resolution and the applied procedure to separate pores in XμCT. The separation of pores depends on the selection of thresholds by the operator and on the actual distance between small pores. The influence of the operator was minimized by iteratively optimizing the thresholds with respect to reducing the sensitivity of the thresholds on the porosity and number of pores. A stronger effect, thus, might be due to pores that are arranged closer to each other than the resolution limit of XμCT (<0.5 μm). Therefore, a cluster of fine pores may be seen as one large pore in XμCT, whereas mercury porosimetry may register every single pore separately. This will result in an overestimation of the larger pores by XμCT.

On the other hand, in mercury porosimetry, a pore-shielding effect may cause an overestimation of fine pores. The need to
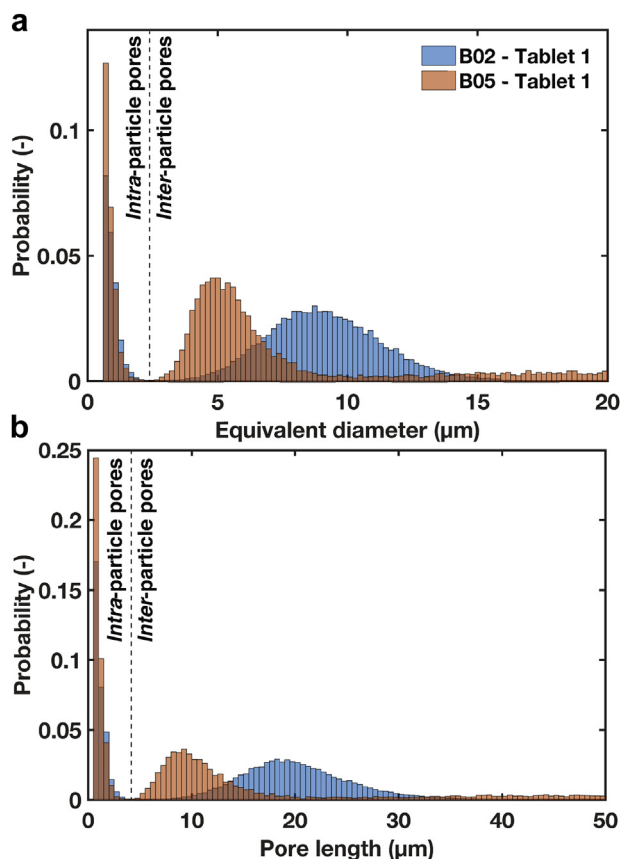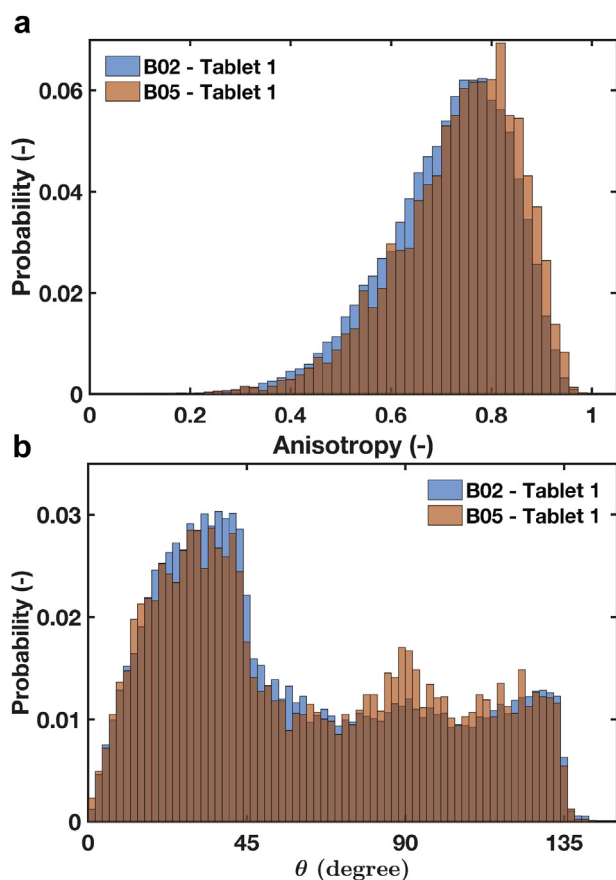
Figure 6. Frequency distribution of (a) the equivalent diameter and (b) the pore length. The separation of the intra- and interparticle pores is highlighted by the vertical dashed line.
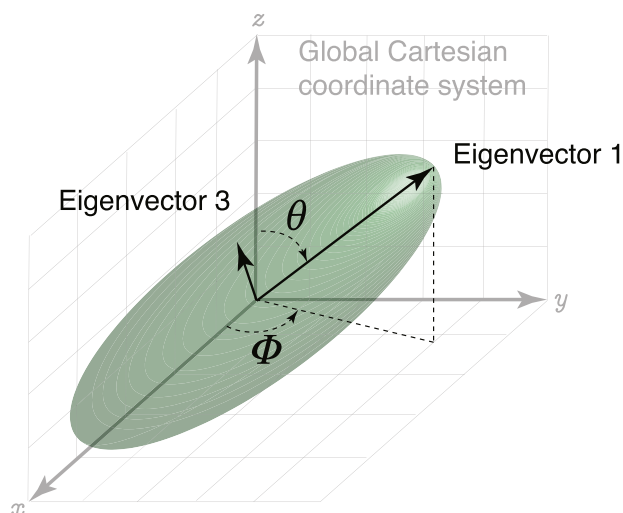
Figure 7. Schematic of a single nonspherical pore described by the eigenvectors. The 3 eigenvectors (only 2 are visualized) are mutually orthogonal to each other and ordered according to its eigenvalue, where the largest eigenvalue corresponds to eigenvector 1 and the smallest to eigenvector 3. The polar angle, θ, and the azimuthal angle, Φ, were calculated for eigenvector 1 and further used to analyze the orientation of the pores. The minimum and maximum eigenvalue, that is, eigenvalue 3 ($\lambda_{\min}$) and 1 ($\lambda_{\max}$) were required to calculate the anisotropy as given in Table 3.

force the nonwetting mercury to break through fine connecting features (throats) between larger pores causes an underestimation of the pore volume associated with the large pores and at the same

Figure 8. Analysis of the anisotropy and orientation of the interparticle pores. Frequency distributions of (a) the anisotropy and (b) the polar angle Θ (calculated from eigenvector 1) for all pores. More details are provided in Figure 7.
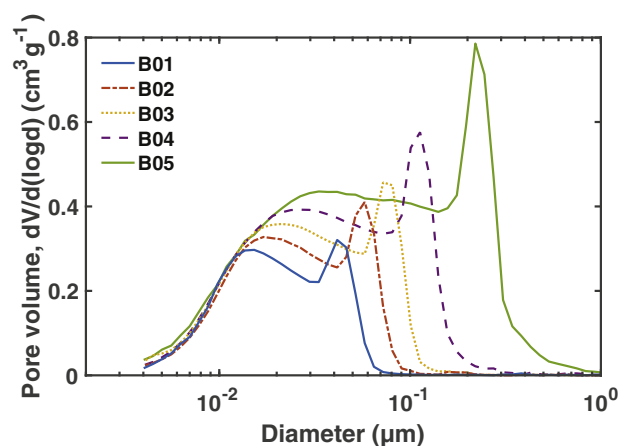
Figure 9. Specific pore volume as a function of pore diameter from mercury porosimetry. One tablet per batch was measured.

time an overestimation of the intrusion volume of the small pores.[30] Although this effect leads to an overestimate of the fine pore sizes, it does not affect the overall porosity.

The mercury porosimetry reveals that the very fine pores remain unchanged as a result of compaction, that is, the specific pore volumes of all batches for pores with a diameter <0.014 μm strongly overlap. This supports our earlier assumption that the intraparticle porosity is not affected by the compaction. Moreover, the compaction of the powder under high pressure also leads to extremely close contact between particles and outer structural elements on the surface of the particles, so it is inevitable that such close contact might lead to pores on a length scale of the intraparticle pores. Consequently, the separable bimodality between inter- and intraparticle pores becomes more questionable under extremely high pressure compaction.
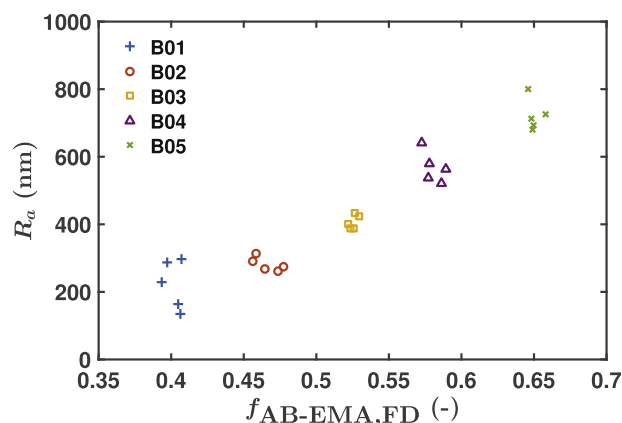
The porosities from mercury porosimetry were compared with the porosity calculated from the density and to that from THz-TDS (Table 4). The porosities from mercury porosimetry are based on the measurement of the bulk density and the true density (skeletal density). The true density was determined for every measurement yielding an averaged value of 2.744 ± 0.126 g cm^{-3} (5 repeats), which was used for the porosity calculations. This true density is slightly lower than that from helium pycnometry (2.958 ± 0.062 g cm^{-3}), which was used to calculate the nominal porosities. Replacing the true density in Equation 1 by the value from mercury porosimetry and using the updated nominal porosities to calibrate the different models (TB-EMA, AB-EMA, and ZPA) for THz-TDS, yields marginally better correlation results for every model than presented in Table 2 (the results are given in the Supporting Information). This suggests that helium pycnometry

Table 4

Comparison of Porosities of the Same Tablets From Mercury Porosimetry, Density Calculations, and THz-TDS (Using n_{eff} From the FD Analysis and the Anisotropic Bruggeman Model)

Batch	Mercury Porosimetry	Porosity via Density Calculations	THz-TDS
		f_{nominal}	$f_{\text{AB-EMA,FD}}$
B01	0.37	0.45	0.44
B02	0.46	0.50	0.50
B03	0.52	0.56	0.56
B04	0.57	0.61	0.60
B05	0.66	0.69	0.68

The density calculations were performed as given in Equation 1 and using the true density from Helium pycnometry ($\varrho_{\text{true}} = 2.958$ g cm^{-3}). The porosities from mercury porosimetry were calculated from the measured bulk and true densities.

Figure 10. Roughness analysis of 5 tablets per batch as a function of the porosity. The porosity was predicted by the AB-EMA using $n_{eff}(1\,Thz)$ from the FD analysis.

overestimates the true density and the estimation from mercury porosimetry may be closer to the real value. An overestimation of the helium pycnometry may be caused by the presence of water molecules in the pore space, which could not be removed before the measurement. The release of the water during the measurement affects the calculation of the skeletal volume, which assumes a constant number of gas molecules, and thus causes an overestimation of the true density.[31]

Roughness Analysis

The roughness was measured for 5 tablets per batch (in total 25 samples). Figure 10 reveals that it linearly depends on the porosity of the tablets, which is in line with previously published studies about MCC tablets.[17] This linear dependence between roughness and porosity is, thus, also valid for such highly porous powder compacts. However, the SD of the measured roughness of B01 is slightly larger than for the other batches, which is not the case for all the other parameters analyzed in this study. Some of the tablets of B01 are even above the average R_a of B02. This may be due to the low interparticle porosity of B01 and B02 leading to the hypothesis that the surface roughness strongly correlates with the interparticle porosity, and it is less affected by the intraparticle porosity.

The linear correlation of R_a and n_{eff} with the porosity provides the scientific basis for future research to analyze the pore structure of a tablet using terahertz technology in a reflection setting. This would be particularly important for cases of strongly absorbing and/or very thick tablets, which cause a low signal-to-noise ratio of the transmitted terahertz pulse leading to an inaccurate effective refractive index. Moreover, determining pore structural properties from reflection measurements may be more practical in an industrial setting as it facilitates an easy process integration.

Conclusion

This work demonstrated the characterization of the pore structure of highly porous FCC tablets by means of THz-TDS and XµCT. XµCT provides highly detailed data about the microstructure of pharmaceutical tablets facilitating the analysis of orientation and shape of every single pore. However, the long acquisition times (several hours) and safety concerns limit the application of this technology for quality control purposes. These limitations can be overcome by terahertz technology, which is a fast, nonionizing, contactless, and nondestructive method. The high potential of this technology to analyze the pore structure was emphasized by an

$R^2 > 0.99$ from the correlation between the porosity predicted from terahertz measurements and the nominal porosity.

Additional information about the pore structure can be extracted on the basis of the S parameter and the depolarization factor. We showed for the first time how this depolarization factor can be used to analyze the shape of pores from terahertz measurement. The results, thus, indicate an anisotropic behavior of the FCC samples which may have impact on critical quality attributes of the solid dosage form. In particular, the high aspect ratio of 1.7 of pores as determined by THz-TDS may have impact on the disintegration of the powder compact by affecting the wicking mechanisms. However, more research is necessary to gain insight into the impact these highly porous tablets with an anisotropic interparticle pore structure have on the disintegration and dissolution performance.

The potential of the terahertz technique to study the dissolution and disintegration performance of immediate release tablets was recently demonstrated by Markl et al.[32] The authors reported a high correlation between the effective refractive index calculated from terahertz measurements and the disintegration time and the API dissolved during the early stage of tablet dissolution. Such a technique is particularly important for tablets containing an API from BCS class II or IV (low solubility), where the dissolution rate can be significantly enhanced by accelerating the liquid penetration using highly porous excipients. However, using models such as TB-EMA or AB-EMA to analyze terahertz data of complex formulations requires a further development of these concepts.

References

1. Desai PM, Liew CV, Heng PWS. Review of disintegrants and the disintegration phenomena. *J Pharm Sci.* 2016;105(9):1-11.
2. Quodbach J, Kleinebudde P. A critical review on tablet disintegration. *Pharm Dev Technol.* 2016;21(6):763-774.
3. Lerk CF, Bolhuis GK, de Boer AH. Effect of microcrystalline cellulose on liquid penetration in and disintegration of directly compressed tablets. *J Pharm Sci.* 1979;68(2):205-211.
4. Yassin S, Goodwin DJ, Anderson A, et al. The disintegration process in microcrystalline cellulose based tablets, Part 1: influence of temperature, porosity and superdisintegrants. *J Pharm Sci.* 2015;104(10):3440-3450.
5. Westermarck S, Juppo AM, Kervinen L, Yliruusi J. Microcrystalline cellulose and its microstructure in pharmaceutical processing. *Eur J Pharm Biopharm.* 1999;48(3):199-206.
6. Bi Y, Sunada H, Yonezawa Y, Danjo K, Otsuka A, Iida K. Preparation and evaluation of a compressed tablet rapidly disintegrating in the oral cavity. *Chem Pharm Bull.* 1996;44(11):2121-2127.
7. Sungthongjeen S, Puttipipatkhachorn S, Paeratakul O, Dashevsky A, Bodmeier R. Development of pulsatile release tablets with swelling and rupturable layers. *J Control Release.* 2004;95(2):147-159.
8. Stirnimann T, Atria S, Schoelkopf J, et al. Compaction of functionalized calcium carbonate, a porous and crystalline microparticulate material with a lamellar surface. *Int J Pharm.* 2014;466(1-2):266-275.
9. Stirnimann T, Di Maiuta N, Gerard DE, Alles R, Huwyler J, Puchkov M. Functionalized calcium carbonate as a novel pharmaceutical excipient for the preparation of orally dispersible Tablets. *Pharm Res.* 2013;30(7):1915-1925.
10. Garnett JCM. Colours in metal glasses and in metallic films. *Philos Trans R Soc A Math Phys Eng Sci.* 1904;203(359-371):385-420.
11. Bruggeman DAG. Berechnung verschiedener physikalischer Konstanten von heterogenen Substanzen. *Annalen der Physik.* 1935;5(24):636-664.
12. Bawuah P, Silfsten P, Ervasti T, Ketolainen J, Zeitler JA, Peiponen KE. Non-contact weight measurement of flat-faced pharmaceutical tablets using terahertz transmission pulse delay measurements. *Int J Pharm.* 2014;476(1-2):16-22.

13. Polder D, Van Santeen JH. The effective permeability of mixtures of solids. *Physica*. 1946;12(5):257-271.

14. Bawuah P, Chakraborty M, Ervasti T, et al. A structure parameter for porous pharmaceutical tablets obtained with the aid of Wiener bounds for effective permittivity and terahertz time-delay measurement. *Int J Pharm*. 2016;506(1-2):87-92.

15. Bawuah P, Tan N, Tweneboah SNA, et al. Terahertz study on porosity and mass fraction of active pharmaceutical ingredient of pharmaceutical tablets. *Eur J Pharm Biopharm*. 2016;105(C):122-133.

16. Spanier JE, Herman IP. Use of hybrid phenomenological and statistical effective-medium theories of dielectric functions to model the infrared reflectance of porous sic films. *Phys Rev B*. 2000;61(15):10437-10450.

17. Bawuah P, Mendia AP, Silfsten P, et al. Detection of porosity of pharmaceutical compacts by terahertz radiation transmission and light reflection measurement techniques. *Int J Pharm*. 2014;465(1-2):70-76.

18. Markl D, Zeitler JA, Rasch C, et al. Analysis of 3D prints by x-ray computed microtomography and terahertz pulsed imaging. *Pharm Res*. 2017 [Epub ahead of print]. http://dx.doi.org/10.1007/s11095-016-2083-1.

19. Seitavuopio P, Rantanen J, Yliruusi J. Tablet surface characterisation by various imaging techniques. *Int J Pharm*. 2003;254(2):281-286.

20. Seitavuopio P, Rantanen J, Yliruusi J. Use of roughness maps in visualisation of surfaces. *Eur J Pharm Biopharm*. 2005;59(2):351-358.

21. Seitavuopio P, Heinämäki J, Rantanen J, Yliruusi J. Monitoring tablet surface roughness during the film coating process. *AAPS Pharm Sci Tech*. 2006;7(2):E1-E6.

22. Jones SB, Friedman SP. Particle shape effects on the effective permittivity of anisotropic or isotropic media consisting of aligned or randomly oriented ellipsoidal particles. *Water Resour Res*. 2000;36(10):2821-2833.

23. Peiponen KE, Vartiainen EM, Unuma T, et al. Dispersion relations for evaluating the complex refractive index of medium without the information of its thickness. *Appl Phys Lett*. 2013;102(18):181110.

24. Hale DK. The physical properties of composite materials. *J Mater Sci*. 1976;11:2105-2141.

25. Tuononen H, Fukunaga K, Kuosmanen M, Ketolainen J, Peiponen KE. Wiener bounds for complex permittivity in terahertz spectroscopy: case study of two-phase pharmaceutical tablets. *Appl Spectrosc*. 2010;64(1):127-131.

26. Akseli I, Hancock BC, Cetinkaya C. Non-destructive determination of anisotropic mechanical properties of pharmaceutical solid dosage forms. *Int J Pharm*. 2009;377(1-2):35-44.

27. Edge S, Steele DF, Tobyn MJ, Staniforth JN, Chen A. Directional bonding in compacted microcrystalline cellulose. *Drug Dev Ind Pharm*. 2001;27(7):613-621.

28. Mullarney MP, Hancock BC. Mechanical property anisotropy of pharmaceutical excipient compacts. *Int J Pharm*. 2006;314(1):9-14.

29. Wu YS, van Vliet LJ, Frijlink HW, Stokroos I, van der Voort Maarschalk K. Pore direction in relation to anisotropy of mechanical strength in a cubic starch compact. *AAPS Pharm Sci Tech*. 2008;9(2):528-535.

30. Gane PAC, Ridgway CJ, Lehtinen E, et al. Comparison of NMR cryoporometry, mercury intrusion porosimetry, and DSC thermoporosimetry in characterizing pore size distributions of compressed finely ground calcium carbonate structures. *Ind Eng Chem Res*. 2004;43(24):7920-7927.

31. Sun CC. A Novel method for deriving true density of pharmaceutical solids including hydrates and water-containing powders. *J Pharm Sci*. 2004;93(3):646-653.

32. Markl D, Sauerwein J, Goodwin DJ, van den Ban S, Zeitler JA. Non-destructive determination of disintegration time and dissolution in immediate release tablets by terahertz transmission measurements. *Pharm Res*. 2017 [Epub ahead of print]. http://dx.doi.org/10.1007/s11095-017-2108-4.